Met. Mater. Int., Vol. 21, No. 3 (2015), pp. 504~510
doi: 10.1007/s12540-015-4400-3

Functional Properties and Morphology of NiTi Articulated Actuation Elements During Thermo-Mechanical Cyclic Tests

Adelaide Nespoli*, Elena Villa, and Francesca Passaretti

Consiglio Nazionale delle Ricerche - Istituto per l'Energetica e le Interfasi (CNR-IENI), Unità di Lecco, Corso Promessi Sposi 29, 23900 Lecco, Italy

(received date: 25 August 2014 / accepted date: 19 December 2014)

Shape memory alloys (SMAs) are active materials able to recover large strains over several thermo-mechanical cycles. In the actuation field, this strain recovery is principally exploited on the mini and micro scales at which SMAs exhibit their highest power density with respect to common lightweight technologies. During the repetitive actuation of a SMA element, certain events occur: strain drift at the beginning of cyclic testing, the accumulation of plastic deformation, and strain stabilisation. In this study, these events as well as the overall mechanical response of an articulated NiTi element were monitored through calorimetry and scanning electron microscopy. Fatigue and cyclic stability were tested under different loads and under different aging conditions. In addition, the surface morphology was continuously observed via scanning electron microscopy to monitor crack growth and propagation during the fatigue test. Finally, before and after the fatigue test, samples were tested through calorimetry to investigate the overall microstructural homogeneity. Results confirm the high potential of the proposed geometry for the development of NiTi non-conventional active elements in the miniature actuation field.

Keywords: shape memory alloys, thermomechanical processing, fatigue, scanning electron microscopy (SEM), differential scanning calorimetry

1. INTRODUCTION

During a thermal loop, shape memory NiTi materials reversibly change their crystalline structure, and they transform into B2 austenite at high temperature and into B19' martensite at low temperature according to a first-order thermoelastic martensitic transformation (TMT) [1,2]. In actuation, the martensite phase undergoes both high deformation and macroscopic shape changes that are recovered during thermal activation. The deformation of the martensite phase is usually achieved by the application of an external load able to promote the re-orientation of martensite variants (de-twinning); during detwinning, the high mobility of the martensite variant interfaces minimises the strain energy and allows for high deformation. The shape recovery obtained after heating de-twinned martensite is normally used to promote mechanical work, and it finds several interesting applications in the field of actuation [3-11].

In many of these applications, the shape that is recovered under a load is exploited to produce linear or rotational motion over a large number of thermo-mechanical cycles. During this training, the accumulation of non-recoverable strain, strain drift and strain stabilisation always occur. The magnitude of these events depends on specific working conditions, such as the applied load, the corresponding recovered strain, the amount of thermal overshoot and the thermo-mechanical history of the alloy. Under certain conditions, the plastic deformation, the strain drift and the overall stroke stabilise after several training cycles. This stabilisation is fundamental to actuation and must be seriously considered during the design of a specific shape memory alloy (SMA) actuator. Furthermore, the fatigue life is another functional property that affects the mechanical response of an actuator [12-22]. This property is related to the strain, the accumulated defects during the cycling process, and the origin of structural changes such as the generation of new stable martensite phases [22]. All these structural modifications cause changes in the transformation temperatures, the thermo-mechanical hysteresis and the fatigue life itself.

The amplitude and number of thermo-mechanical cycles associated with a fatigue route are strictly related to several practical factors: the quality of the alloy (i.e., the presence and amount of defects such as titanium carbide inclusions after melting [23] and precipitates after annealing), the geometry of the SMA element, the shape and the orientation during normal functioning (vertical or horizontal, [24]), the applied load and corresponding strain, the heating source parameters

*Corresponding author: a.nespoli@ieni.cnr.it

and the environmental temperature relative to the characteristic transformation temperature of the material. Hence, the optimisation of the thermo-mechanical response of a SMA actuator often derives from a balance between these practical factors and the desired functional output.

SMAs are commonly employed as actuators in the form of straight wires or helical springs. In previous studies [25,26], an uncommon snake-like geometry has been proposed as a possible alternative to the wire and spring shapes, especially in confined spaces.

Under low loads, the strain of the snake-like element derives and depends only on the bending-unbending movement of the element's curves. In fact, for an optimal working condition and to avoid uncontrolled plastic deformation, only the curved parts of the snake-like element should work, and less than a few tens of degrees of deformation is always recommendable. Under these conditions, the bending-unbending motion of the curves of the snake-like element during cycling causes the corresponding fibres to continuously undergo compression and tension. Hence, for a high number of thermo-mechanical cycles, the curved parts are the mechanically weakest points of the snake-like element.

In this work, we present an experimental study on the thermo-mechanical cyclic response of an articulated snake-like SMA element. Fatigue and cyclic stability were tested under different loads and under different annealing conditions. In addition, the morphology of the surface of the element's curves were continuously observed via scanning electron microscopy to monitor crack growth and propagation during the fatigue test. Finally, calorimetry was used to test the microstructural homogeneity of the material before and after the fatigue analysis.

2. EXPERIMENTAL PROCEDURE

Several articulated SMA samples were prepared from a cold-worked NiTi commercial wire (0.2 mm diameter). To promote the shape memory effect, two types of hot-forming procedures were considered, one conducted at 450 °C and the other at 500 °C, both of them with a duration of 10 minutes, which were followed by quenching in water at room temperature. During the hot shaping, the SMA wire was formed into the four-curve snake-like geometry described in [25] and depicted in Fig. 1.

Calorimetry (DSC, Seiko 220C equipped with a nitrogen cooling system) was employed to evaluate the phase transformation temperatures over the range of -40 °C to 80 °C at a heating/cooling rate of 10 °C/min. The DSC response was also used to verify the homogeneity of the microstructure that the alloy presented before and after the thermo-mechanical fatigue tests.

Cyclic tests were performed under constant loads of 0.1 N and 0.2 N, whereas the fatigue life was studied only under a load of 0.1 N. During these tests, the stroke was registered using a linear variable displacement transducer (LVDT, DC50 Solartron Metrology), and the snake-like element was heated by the Joule effect (0.6 A for 3 s); the cooling/reset time was set to 7 seconds.

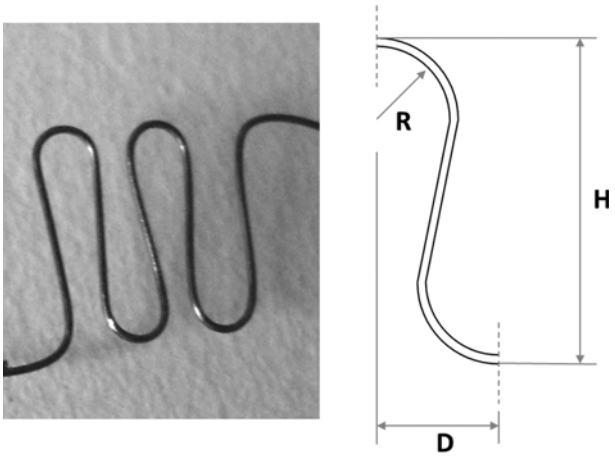

Fig. 1. Photograph of the articulated snake-like sample (H=5.27±0.07 mm, R=0.54±0.03 mm, D=0.82±0.06 mm, number of curves = 4) [24].

In addition, strain recovery curves were registered for the same sample during the fatigue analysis. For this purpose, strain recovery curves were recorded at various pre-selected fatigue cycles (1st, 5th, 10th, 100th, 500th, 10^3th, and 10^4th). The test was executed using a standard tensile testing machine (DMA, Q800 TA Instruments) under a constant load of 0.1 N over the temperature range of -80 °C to 150 °C at a heating/cooling rate of 5 °C/min. At the same time, the change in the sample surface morphology during fatigue was analysed through scanning electron microscopy (SEM LEO 1430) observations after 10^3 and 10^4 fatigue cycles and after fracture.

3. RESULTS AND DISCUSSION

In this work, a set of experimental investigations highlighted different effects of cyclic load tests on a snake-shaped SMA element. All discussed aspects are currently under consideration through numerical analysis; however, the series of functional, calorimetric and microscopic analyses provided information that depicts, in great detail, the effects of fatigue on the actuator element tested.

Before carrying out cyclic tests, a NiTi snake-like sample was analysed through DSC to evaluate the overall microstructural homogeneity of the shaped SMA wire conferred by the hot-forming process. Within this context, particular attention was paid to the calorimetric response of the curved and straight parts of the snake-like element that were separately tested. The calorimetric thermograms of these two sets of parts are reported in Fig. 2. It can be observed that the two curves overlap; that is, the material microstructure is nearly homogeneous

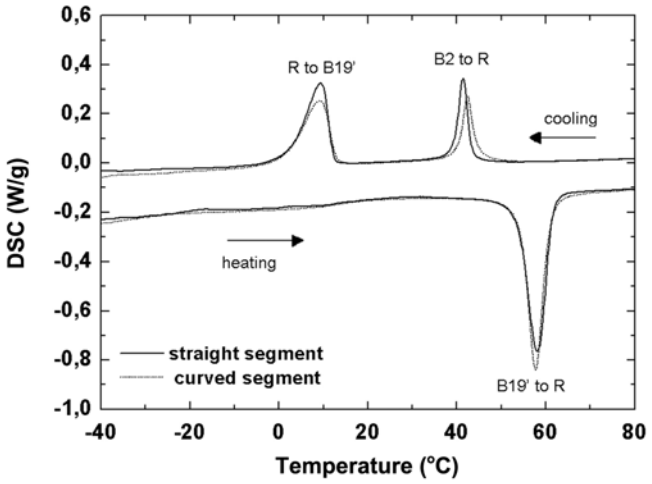

Fig. 2. DSC graphs of the curved (broken line) and straight (solid line) segments of a single SMA element before the cycling test.

throughout the entire length of the snake-like element. The phase transformation temperatures and the transformation enthalpy of the snake-like element before the cyclic test are reported in Table 1.

With respect to the cyclic functional tests, it is worth noting that they were mainly focused on verifying the two stable microstructures that were obtained by the two thermal treatments described in the experimental section. To this end, 10^4 cyclic stability tests under loads of 0.1 N and 0.2 N were performed; the results are reported in Fig. 3. It can be observed that all specimens showed good cyclic stability. In fact, the strokes stabilised within a few hundred actuation cycles for all specimens. In particular, it can be observed that the initial drift of the stroke of the samples treated at 500 °C stabilised earlier than that of the samples treated at 450 °C. Furthermore, the cyclic stability of the sample treated at 500 °C does not appear to have depended on the applied load. In contrast, it

Table 1. Phase transformation temperatures and transformation enthalpy upon cooling and upon heating of the snake-like element before the cycling test (R, M, and A indicate the rhombohedral, martensite and austenite phase transformation temperatures, respectively; s, p, and f indicate the starting, peak and finishing points, respectively)

COOLING	R_s °C	R_p °C	R_f °C	M_s °C	M_p °C	M_f °C	ΔH cooling J/g
not cycled	48.3	45.9	42.8	2.9	-1.9	-15.6	-19.6
HEATING	R_s °C	R_p °C	R_f °C	A_s °C	A_p °C	A_f °C	ΔH heating J/g
not cycled	-	-	-	49.4	55	60	22.5

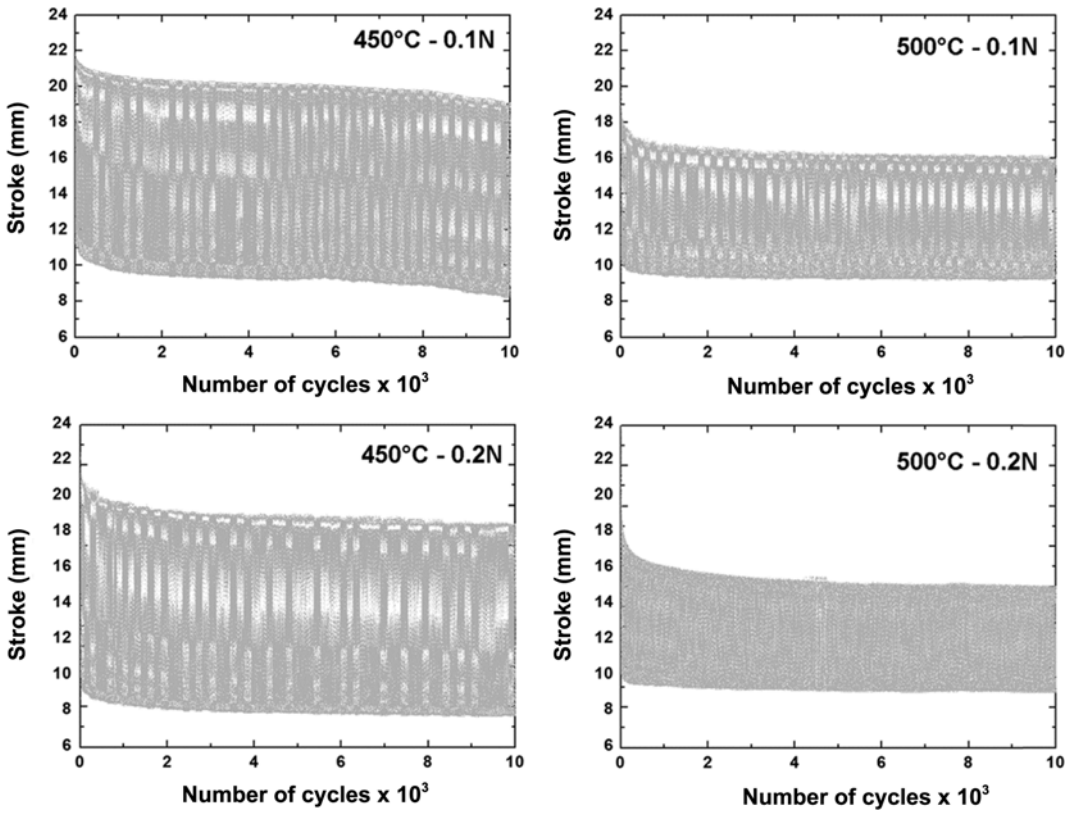

Fig. 3. Evolution of the absolute stroke during the 10^4 cycling test under loads of 0.1 N and 0.2 N for the SMA samples treated at 450 °C and 500 °C for 10 minutes and quenched in water at room temperature.

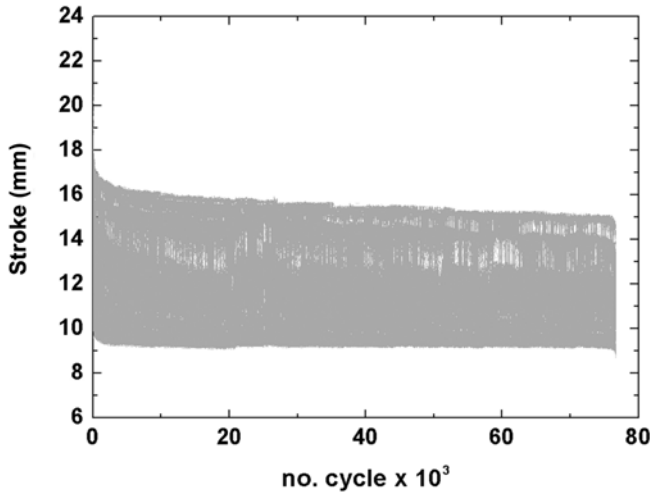

Fig. 4. Fatigue of the sample treated at 500°C under a load of 0.1 N.

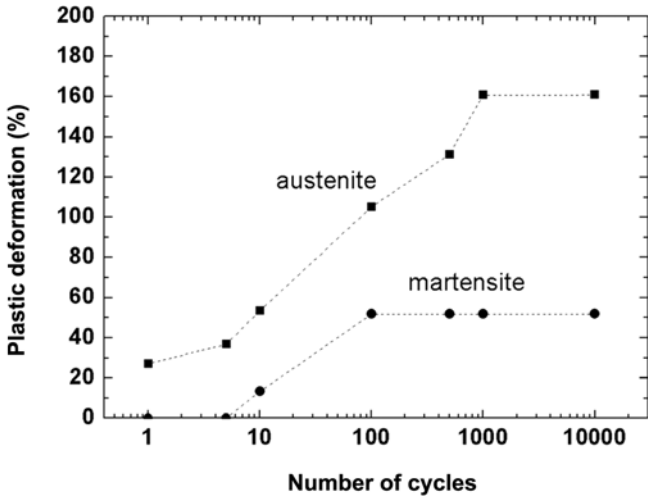

Fig. 6. Plastic deformation of martensite and austenite phases of the snake-like sample accumulated during the fatigue test.

can be observed that the sample treated at 450 °C shows a second marked drift of the stroke after approximately 6×10^3 cycles under a load of 0.1 N. This double drift may be related to the involvement of different regions of martensite during the recovery process. The double drift disappeared when the external load was increased to 0.2 N. In addition, despite its cyclic instability, the samples treated at 450 °C presented the most highly stabilised stroke.

Based on the cyclic test results, the focus of the fatigue analysis was directed toward the snake-like sample that was thermally treated at the highest temperature. Figure 4 shows the fatigue life of a sample treated at 500 °C under a load of 0.1 N. Fracture occurred at the apex of the curve located farthest from the applied load at approximately the 75×10^3th cycle. During the fatigue study, the test was periodically interrupted to produce a slow thermal hysteresis loop under the constant 0.1 N load (Fig. 5). In Figure 5, several mechanical effects of the cyclic procedure can be observed. First, the stroke stabilises near the 10^3th cycle. Simultaneously, during the test, the snake-like element gradually accumulated a certain amount of plastic deformation (Fig. 6). In particular, it can be observed that the amount of plastic deformation sustained by the austenite phase differs from that sustained by the martensite one: approximately 10 mm for the austenite and approximately 2.5 mm for the martensite. This discrepancy is likely due to the defects induced by the thermo-mechanical cycling that hindered the complete recovery of the austenitic phase at high temperatures and drove the two-way shape memory effect [10] in the martensite, reducing the measured plastic deformation at lower temperatures. Furthermore, the thermal hysteresis decreased with the increase in the number of cycles (see also Fig. 7) due to the stabilisation of the thermoelastic martensitic transformation. At the same time, the accumulation of the two-way shape memory effect (TWSME) was precisely registered by imposing a stress-free thermal hyster-

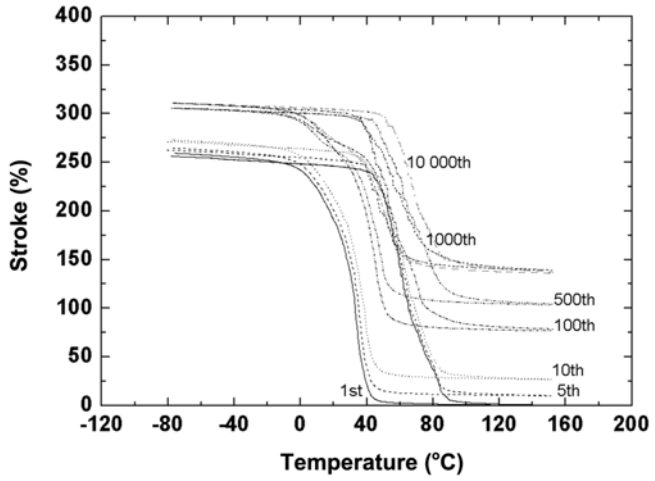

Fig. 5. Strain recovery curves under a load of 0.1 N for the sample treated at 500 °C after the 1st, 5th, 10th, 100th, 500th, 10^3th, 10^4th fatigue cycles.

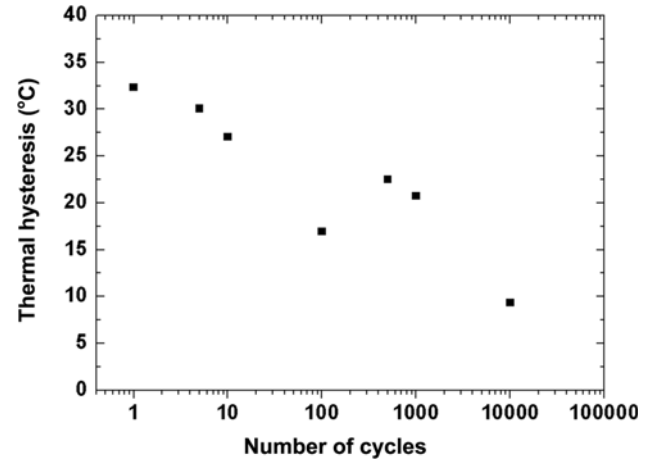

Fig. 7. Thermal hysteresis of the snake-like sample during the fatigue test.

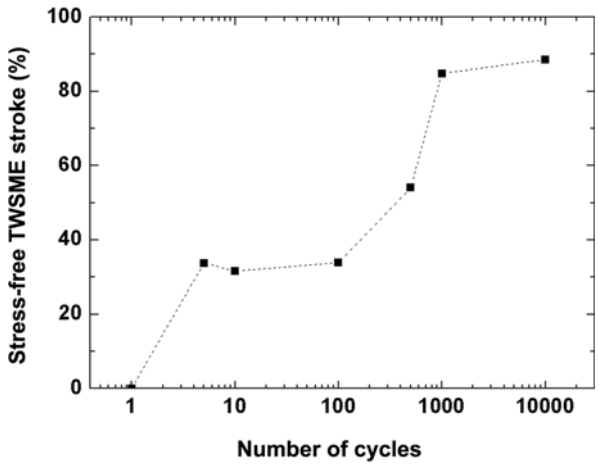

Fig. 8. Two-way shape memory effect (TWSME) stroke of the snake-like sample accumulated during the fatigue test.

esis loop. Figure 8 shows that after the 10^3th cycle, the TWSME stroke stabilised to 6 mm.

A detailed SEM investigation was carried out to control and verify the morphology of the materials and to localise the principal sites of degradation of the materials' structure.

The surface quality of the materials during the fatigue tests is depicted in the SEM images reported in Figs. 9-11. Figure

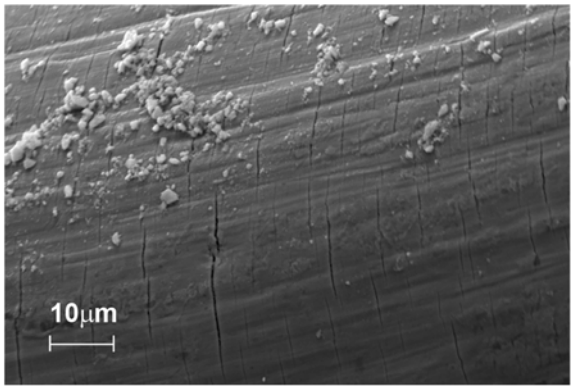

Fig. 11. SEM images of the longitudinal surface of a fractured snake-like sample.

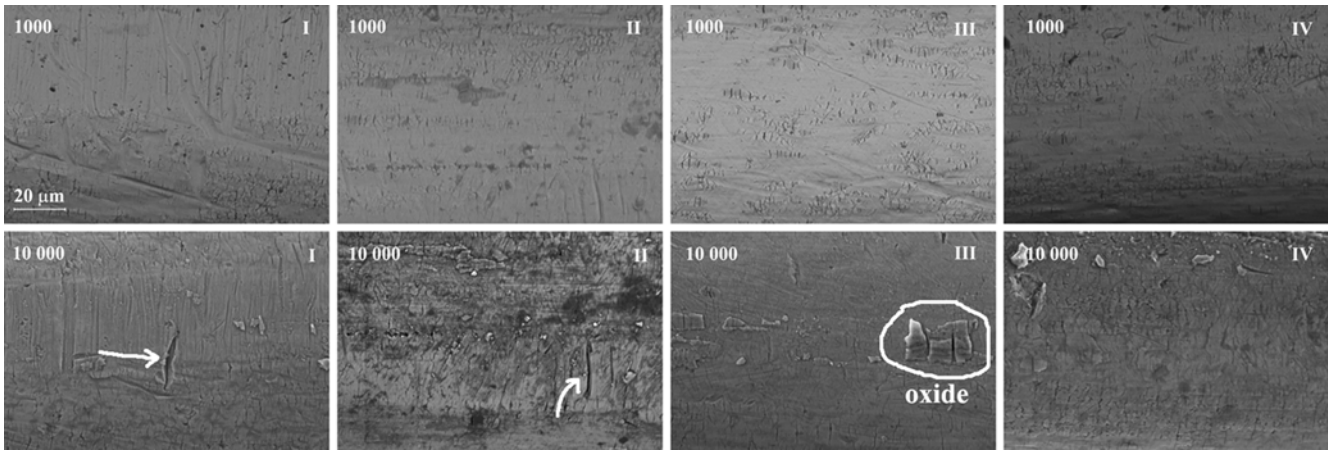

Fig. 9. SEM images of the central inner part of the four curves after 10^3 and 10^4 cycles of the fatigue test. Arrows indicate the cracks that initiated during the fatigue test.

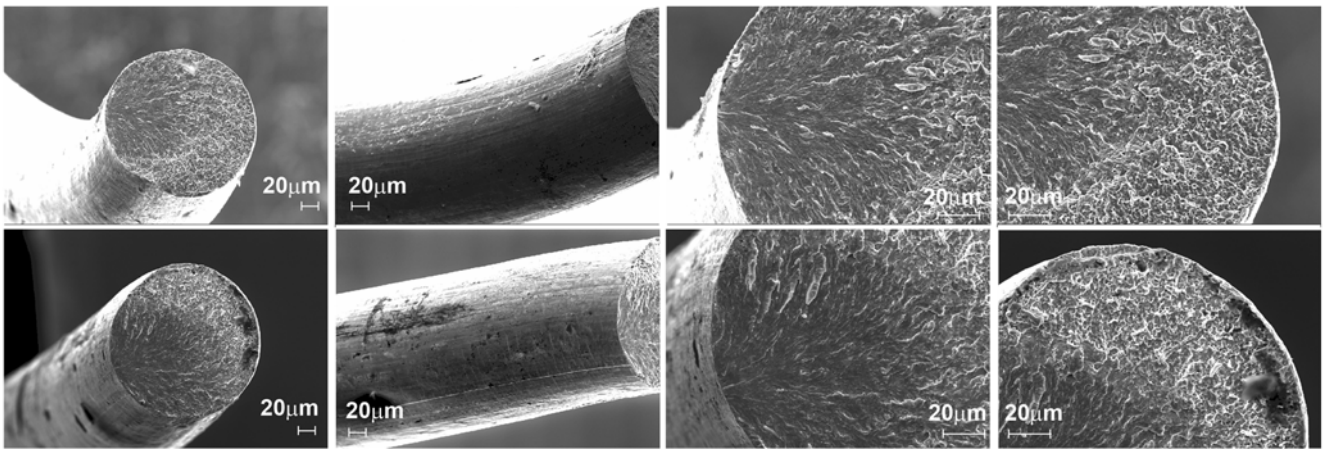

Fig. 10. SEM images of the surfaces of the fractured curves.

Table 2. Phase transformation temperatures and transformation enthalpy upon cooling and upon heating of the snake-like element after the cycling test (P1, P2, P3, P4, and P5 refer to the transformation temperatures of new peaks; s, p, and f indicate the starting, peak and finishing points, respectively)

COOLING	P1_s °C	P1_p °C	P1_f °C	P2_s °C	P2_p °C	P2_f °C	P3_s °C	P3_p °C	P3_f °C	ΔH cooling J/g
cycled curvature	48.6	45.1	-	-	37.7	29.7	7	2.1	-8.3	-22.47
cycled straight part	46.9	44.9	42	-	37	-	6.2	1.7	-14.2	-28.6

HEATING	P4_s °C	P4_p °C	P4_f °C	P5_s °C	P5_p °C	P5_f °C	ΔH heating J/g
cycled curvature	49.6	54.8	-	-	64	66.1	19.24
cycled straight part	49.6	55.4	-	-	64.4	65.9	19.24

9 shows that after 10^3 cycles, the inner part of the four curves did not present macroscopic damages. Thus, the four curves showed similar surface quality. The micrometre-sized fissures visible on the surface represent the breaking of the thin oxide layer due to continuous cycling.

A second set of SEM images was obtained after 10^4 cycles; the images show that the curves located farthest from the applied load (the first and the second ones) presented small cracks measuring approximately 20 μm, whereas the other two did not show any fractures. This behaviour was principally due to the asymmetry of the snake-like sample that originated from the different distributions of momentum along the four curves. Based on this conjecture, the first curve (which was located farthest from the applied load) underwent the highest extent of mechanical cycling. This aspect will be confirmed by the simulations of the stress and momentum distributions over this snake-like geometry that are currently under consideration.

Figure 10 and Fig. 11 show the sample surface after rupture. The fractured section in Fig. 10 shows a region with a striation due to crack propagation from a nucleation site located on the inner surface of the snake-like element. Far from the nucleation site, a second characteristic region can be observed; the region is full of micro-voids and dimples, which are typical defects of ductile materials. Several cracks are also visible on the lateral surface near the fractured section (Fig. 11).

The DSC results obtained for the sample after cyclic testing are reported in Fig. 12 and Table 2. Again, DSC was performed on the curved and straight parts of the element separately. The DSC scan shows that after the fatigue test, these two sets of parts exhibited different calorimetric responses. In particular, the curved segments showed both austenite-to-rhombohedral (B2 to R) and martensite-to-austenite (B19' to A) peaks. This phenomenon occurred due to the introduction of structural changes in the form of defects and the formation of new martensite domains, both consequences of thermo-mechanical cycling. On the other hand, the straight segments only showed a shift in the transformation peaks, which is a typical effect of thermal cycling (also observed for the curved parts), confirming that the straight segments only serve as stroke amplifiers.

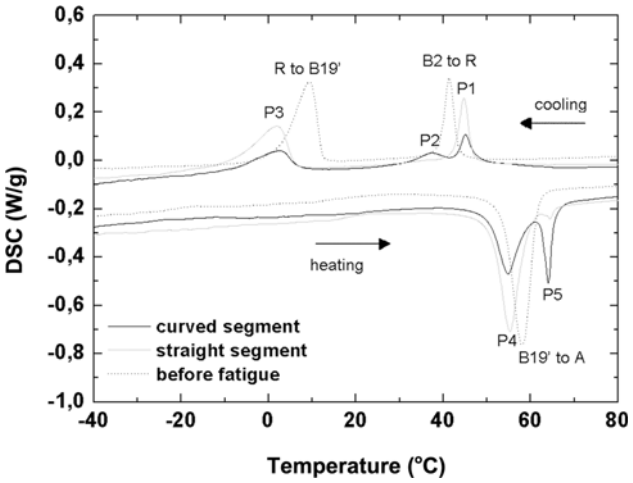

Fig. 12. DSC curves before the fatigue test (dotted line) and after fracture (the black line represents curved segments, and the grey line represents straight segments).

5. CONCLUSIONS

This work presents the results of an experimental investigation of the thermo-mechanical response of snake-like NiTi samples during cyclic testing. Calorimetry confirms that for small strains, the curved parts of the samples are most affected by mechanical cycling. Moreover, SEM observations show that fracture initiates from the curves located farthest from the applied load. Under a load of 0.1 N, the stroke stabilises after 10^3 cycles, as do the plastic deformation and the two-way shape memory effect.

REFERENCES

1. H. Funakubo, *Shape Memory Alloys*, pp.8-23, Gordon & Breach Science Publishers (1984).
2. K. Otsuka and C. M. Wayman, *Shape Memory Materials*, pp.27-48, Cambridge University Press (1998).
3. A. Nespoli, S. Besseghini, S. Pittaccio, E. Villa, and S. Viscuso, *Sens. Actuators A* **158**, 149 (2010).
4. J. M. Jani, M. Leary, A. Subic, and M. A. Gibson, *Mater. Design* **56**, 1078 (2014).

5. I. Y. Young, W. J. Ju, H. L. Jae, K. Kyung-Won, H. Do-Soon, and J. L. Jung, *Rev. Sci. Instrum*. **84**, 015005 (2013).
6. L. Chih-Ming, C. Cheng-Yu, and L. Chao-Chieh, *Smart Mater. Struct*. **22**, 08500 (2013).
7. A. Lara-Quintanilla, A. W. Hulskamp, and H. E. N. Bersee, *J. of Intel. Mater. Syst. Struct*. **25**, 2246 (2014).
8. H. K. Jeong, J. H. Han, S. H. Youn, and J. Lee, *J. Intel. Mater. Syst. Struct.* **25**, 908 (2014).
9. T. Matsunaga, K. Totsu, M. Esashi, and Y. Haga, *Display* **34**, 89 (2013).
10. A. Nespoli, D. Rigamonti, E. Villa, and F. Passaretti, *Sen. Actuators A* **218**, 142 (2014).
11. A. Nespoli, V. Dallolio, F. Stortiero, S. Besseghini, F. Passaretti, and E. Villa, *Mater. Sci. Eng*. C **37**, 171 (2014).
12. G. Scirè Mammano and E. Dragoni, *Int. J. Fatigue* **69**, 71 (2014).
13. D. C. Lagoudas, D. A Miller, L. Rong, and P. K. Kumar, *Smart Mater. Struct*. **18**, 085021 (2009).
14. O.W. Bertacchini, D.C. Lagoudas, and E. Patoor, *Proc. SPIE 5053, Smart Structures and Materials 2003: Active Materials: Behavior and Mechanics*, p.612, SPIE, San Diego, USA (2003).
15. E. Hornbogen, *J. Mater. Sci*. **39**, 385 (2004).
16. S. Miyazaki, K. Mizukoshi, T. Ueki, T. Sakuma, and Y. Liu, *Mater. Sci. Eng. A* **273-275**, 658 (1999).
17. A. R. Pelton, G. H. Huang, P. Moine, and R. Sinclair, *Mater. Sci. Eng. A* **532**, 13 (2012).
18. C. Dunand-Châtellet and Z. Moummi, *Int. J. Fatigue* **36**, 163 (2012).
19. G. Eggeler, E. Hornbogen, A. Yawny, A. Heckmann, and M. Wagner, *Mater. Sci. Eng. A* **378**, 24 (2004).
20. K. M. Melton and O. Mercier, *Acta Metall. Mater.* **27**, 137 (1979).
21. K. Gall, J. Tyber, G. Wilkesanders, S.W. Robertson, R.O. Ritchie, and H.J. Maier, *Mater. Sci. Eng. A* **486**, 389 (2008).
22. J. Van Humbeeck, *J. de Physique* IV **1**, 189 (1991).
23. M. Rahim, J. Frenzel, M. Frotscher, J. Pfetzing-Micklich, R. Steegmüller, M. Wohlschlögel, H. Mughrabi, and G. Eggeler, *Acta Mater.* **61**, 3667 (2013).
24. C. Zanotti, P. Giuliani, S. Arnaboldi, and A. Tuissi, *Proc. SMST-2010 Global Solutions for Future Applications*, p.688, Springer, New York (2011).
25. A. Nespoli, E. Villa, and S. Besseghini, *J. Therm. Anal. Calorim*. **109**, 39 (2012).
26. A. Nespoli, E. Bassani, S. Besseghini, and E. Villa, *Physics Procedia* **10**, 182 (2010).